Published in final edited form as:
Arterioscler Thromb Vasc Biol. 2011 April ; 31(4): 750–757. doi:10.1161/ATVBAHA.110.221499.

Detection of macrophages in aortic aneurysms by nanoparticle PET-CT

Matthias Nahrendorf, MD, PhD*, **Edmund Keliher, PhD***, **Brett Marinelli, BA**, **Florian Leuschner, MD**, **Clinton S. Robins, PhD**, **Robert E. Gerszten, MD**, **Mikael J. Pittet, PhD**, **Filip K. Swirski, PhD**, and **Ralph Weissleder, MD, PhD**
Center for Systems Biology, Massachusetts General Hospital and Harvard Medical School, Simches Research Building, 185 Cambridge St., Boston, MA 02114

Abstract

Objective—Current management of aortic aneurysms (AAs) primarily relies on size criteria to determine whether invasive repair is indicated to preempt rupture. We hypothesized that emerging molecular imaging tools could be used to more sensitively gauge local inflammation. Since macrophages are key effector cells that destabilize the extracellular matrix in the arterial wall, it seemed likely that they would represent suitable imaging targets. We here aimed to develop and validate macrophage-targeted nanoparticles labeled with fluorine-18 (^{18}F) for PET-CT detection of inflammation in AAs.

Methods and Results—Aneurysms were induced in apoE$^{-/-}$ mice via systemic administration of angiotensin-II. Mice were imaged using PET-CT and a monocyte/macrophage-targeted nanoparticle. AAs were detected by contrast-enhanced micro-CT and had a mean diameter of 1.85 ± 0.08 mm, whereas normal aortas measured 1.07 ± 0.03 ($p < 0.05$). The in vivo PET signal was significantly higher in aneurysms (SUV 2.46 ± 0.48) when compared to wild type aorta (0.82 ± 0.05, $p<0.05$). Validation with scintillation counting, autoradiography, fluorescence and immunoreactive histology and flow cytometry demonstrated that nanoparticles predominantly localized to monocytes and macrophages within the aneurysmatic wall.

Conclusions—PET-CT imaging with ^{18}F-CLIO (cross-linked iron oxide) nanoparticles allows quantitation of macrophage content in a mouse model of AAs.

Keywords

Aortic aneurysm; inflammation; macrophage; PET-CT; nanoparticle

Introduction

The prevalence of aortic aneurysms in the elderly population is approximately 5%[1]. Up to 50% of larger aneurysms rupture,[1] an event that carries a mortality rate of around 50%[2]. The current management strategy for patients with aneurysms includes a combination of anatomical imaging, watchful waiting and surgical intervention to preempt deadly ruptures. Decision to intervene surgically depends on the size and location of the aneurysm: a rapidly increasing size or a diameter above 5.5 cm is considered an indication for intervention. If lower diameters are encountered, repeated monitoring with anatomical imaging is

Corresponding author: Matthias Nahrendorf or Ralph Weissleder, Center for Systems Biology, 185 Cambridge Street, Boston, MA 02114, Tel: (617) 643-0500, Fax: (617) 643-6133, mnahrendorf@mgh.harvard.edu, rweissleder@mgh.harvard.edu.

Conflict of Interest Disclosures
None.

recommended[1,3,4]. The timing of therapy and imaging is difficult but crucial, since both invasive repair and progressive disease carry significant risks. Smaller aneurysms may rupture between successive scheduled imaging sessions, while some large but relatively stable aneurysms are operated on, exposing patients to unnecessary risks. There is, therefore, a need for better risk prediction in order to personalize strategies for individual patients.

Insight into the pathobiology of aneurysms is evolving quickly, and increasing evidence points to an important role for innate immune cells[5,6]. Monocytes/macrophages infiltrate the vessel wall and release proteases, among them elastase and metalloproteinases, that compromise the integrity of the vascular wall through degradation of the extracellular matrix. Monocytes/ macrophages also secrete inflammatory cytokines in the media and adventitia of aneurysmatic vessels, such as TNFα, IFNγ and IL-6[7,8]. These inflammatory processes precede the increase in vessel diameter and are involved in aneurysm growth and rupture in animal models[5,7,9]. Therefore, imaging of macrophage presence and function in a vascular domain may report on the propensity of an aneurysm to rupture earlier and with greater specificity than methods that focus on anatomy. In this investigation, we hypothesized that nanoparticles targeted to macrophages could be used to detect inflammation in aortic aneurysms using imaging methods. We used nanoparticle-based PET reporters that can be detected at trace concentrations, and which are analogous to nanoparticles recently approved by the FDA (Feraheme©). The coating and size of the nanoparticles were optimized to target monocytes/macrophages[10,11]. In addition, recently developed PET isotope labeling strategies using “click” chemistry[12] allowed for rapid labeling of nanoparticles with the widely-used clinical PET tracer, fluorine-18 (^{18}F). PET-CT is a preeminent choice of modality for this application since it combines the superior sensitivity of quantitative PET imaging with high-resolution anatomical information derived from CT. Nanoparticles used in this study were co-labeled with fluorochromes to facilitate the validation of agent location with optical imaging techniques.

Methods

Animal models

In this investigation, apoE$^{-/-}$ mice were systemically administered with angiotensin-II (AT-II) over a prolonged period[13,14]. This model system was chosen because of the presence of atherosclerosis, a shared common risk factor with human patients[15]. Even more importantly, this model resembles the clinical situation in that aneurysm rupture is a documented complication[16]. For aneurysm induction, apoE$^{-/-}$ mice were subcutaneously implanted with osmotic minipumps (Alzet, 2004) releasing 1μg/min/kg AT-II (Bachem) for 28 days (n=16) or 7 days (n=19). Minipumps were pre-incubated in PBS for 4 hours to assure immediate delivery of the agent after implantation. At the time of implantation, apoE$^{-/-}$ mice were 6 months old, and had been kept on a high cholesterol diet (Harlan). Female apoE$^{-/-}$ mice and C57BL/6J controls (n=14) were purchased from Jackson Labs.

In one subgroup of mice, the splenic monocyte reservoir was surgically removed in order to modulate the supply of monocytes, and consequently the number of their lineage descendant macrophages in the aortic wall. In previous work, it had been shown that the spleen contains a large population of undifferentiated monocytes, and that these cells are released into the blood pool upon AT-II administration. It was subsequently shown that splenic monocytes can contribute up to ~50% of the myeloid cells in inflamed tissue[17,18]. To surgically remove the spleen, animals were anesthetized in an isoflurane chamber at 2L/min O_2 at 2% concentration. Under anesthesia, the abdominal cavity of the mice was opened in the left upper quadrant. The spleen was gently exteriorized and the splenic artery and vein were cauterized. The spleen was then removed, and the peritoneum and skin were then closed using ETHICON 6-0 Ethilon suture.

Nanoparticle preparation

Dextran coated iron oxide nanoparticles (CLIO-47, Center for Systems Biology, Boston, MA) served as the starting materials. The dextran coating of the nanoparticle was crosslinked with epichlorin hydrin, aminated and labeled with a near infrared fluorochrome (a method we have used previously; VT680, VisEn Medical, Bedford, MA), to render particles fluorescent[11]. The ratio of VT680 per nanoparticle was approximately 5 fluorochromes/particle. The copper-catalyzed azide/alkyne 'click' labeling strategy was employed for ^{18}F-labeling of nanoparticles[11]. Briefly, cross-linked iron oxide (CLIO) nanoparticles were derivatized with alkyne, and the click partner azide was attached to an ^{18}F-labeled polyethylene glycol (^{18}F-PEG$_3$N$_3$). Amidation of aminated CLIO with N-succinimidyl 4-pentynoate was performed as described previously[10]. Following size exclusion chromatography, the concentration of the alkyne-modified CLIO solutions was 1 mg/100 μL. 1-Azido-2-(2-(2-^{12}-fluoroethoxy)ethoxy)ethane (^{18}F-PEG$_3$N$_3$) was prepared from 2-(2-(2-azidoethoxy)ethoxy)ethyl *p*-toluenesulfonate in 51 ± 5% (n=15) average decay-corrected radiochemical yield. Analytical HPLC demonstrated >99% radiochemical purity of ^{18}F-PEG$_3$N$_3$. Finally, ^{18}F-PEG$_3$-N$_3$ was conjugated to alkyne-modified CLIO nanoparticles using click chemistry[12]. Following size exclusion chromatography using a PD-10 column (GE Biosciences, Piscataway, NJ), the final solution of ^{18}F-CLIO was 0.25 mg/100 μL in 1xPBS, and HPLC analysis demonstrated that ^{18}F-CLIO was >98% radiochemically pure. The mean specific activity was 677.1 ± 81.4 MBq/mg Fe.

PET-CT

Mice were imaged with PET-CT using an Inveon small animal scanner (Siemens). Initially, 4 dynamic scans were performed over several hours to determine the best imaging time point after intravenous nanoparticle injection. A high resolution Fourier rebinning algorithm was used to rebin sinograms, followed by a filtered back-projection algorithm to reconstruct three-dimensional images without attenuation correction. Isotropic mage voxel size was 0.796 × 0.861 × 0.861 mm, for a total of 128 × 128 × 159 voxels. Peak sensitivity of the Inveon accounts for 11.1% of positron emission with a mean resolution of 1.65 mm[19]. More than 100 counts were acquired per pixel and the average signal to noise ratio was greater than 20. Calibration of the PET signal with a cylindrical phantom containing ^{18}F isotope was performed prior to all scans. Data are expressed as mean standard uptake values (SUV), which normalizes activity for body weight and injected activity. Target to background ratios (TBR) were calculated in regions of interest to account for contribution of blood signal. A mean activity of 77.7 ± 5.6 MBq in 60 ± 10 μL was injected through the tail vein in mice with an average weight of 22.8 ± 0.83 g.

CT images were reconstructed from 360 cone-beam x-ray projections with a power of 80keV and 500 μA. The isotropic resolution of the CT images was 60 μm. During CT acquisition, iodine contrast was infused into the tail vein at a rate of 35 μl/min to enhance intravascular contrast. Projections were acquired at end expiration using a BioVet gating system (M2M Imaging, Cleveland, OH) and the CT acquisition time was ~10 minutes. Reconstruction of data sets, PET-CT fusion and image analysis were done using IRW software (Siemens). Three-dimensional visualizations were produced using the DICOM viewer OsiriX (The OsiriX foundation, Geneva, Switzerland).

Ex vivo tissue imaging

All mice were placed in a well counter (CRC-127R, Capintec, Ramsey, NJ) after injection and again before dissection, to record total corporeal activity. Aortas were then excised using a surgical microscope and micro-dissection tools, and radioactivity was measured using a gamma counter (1480 Wizard 3″, PerkinElmer, Boston, MA). Finally, tissues were exposed over night for digital autoradiography, and plates were analyzed using a Typhoon

scanner (GE). Six aortas were also imaged with a surface reflectance fluorescence microscope (OV-100, Olympus) to detect signal from the fluorochrome on the nanoparticles.

Histology

Aorta histology was assessed in mice with aneurysms, which had been sacrificed 28 days after minipump (delivering AT-II) implantation, and 24 hours after injection of a cold version of the nanoparticle. Aortas were excised, rinsed in PBS and embedded in OCT compound (Sakura Finetek). Fresh-frozen 6μm-thick serial sections were stained with H&E, as well as immunohistochemically for detection of macrophages. The primary antibody was MAC-3, followed by a secondary antibody (both BD Pharmingen) and avidin-biotin peroxidase. The reaction was visualized using a 3-amino-9-ethyl-carbazol substrate (AEC, DAKO California). On adjacent sections, we analyzed microscopic nanoparticle distribution with a Nikon 80i upright fluorescence scope equipped with a CCD camera connected to a Macintosh workstation.

Flow cytometry

Flow cytometry experiments were conducted in duplicate on cell suspensions retrieved from excised aortas in order to assess the cellular probe distribution and the number of infiltrating leukocytes in different groups[20]. A total of 8 mice were used: 2 apoE$^{-/-}$ mice with and without splenectomy, 7 days after minipump implantation, and 24 hours after injection of 5 mg/kg bodyweight of a cold version of the nanoparticle preparation; 2 wild type mice 24 hours after probe injection; and 2 wild type mice without probe injection as a background/ autofluorescence control. The entire aorta from each mouse was harvested, minced with fine scissors, and placed into a cocktail of collagenase I, collagenase XI, DNase I, and hyaluronidase (Sigma-Aldrich) and shaken at 37°C for 1 hour. Cells were then triturated through a nylon mesh and centrifuged (15 minutes, 500g, 4°C). Total cell numbers were determined with Trypan blue (Mediatech, Inc.). The following antibodies were used to stain the cell suspensions retrieved from the aortas: anti–CD90-PE, 53-2.1 (BD Biosciences, San Jose, Calif); anti–B220-PE, RA3-6B2 (BD Biosciences); anti–CD49b-PE, DX5 (BD Biosciences); anti–NK1.1-PE, PK136 (BD Biosciences); anti–Ly-6G-PE; anti-Ly6C-FITC; anti-CD11b-APC-Cy7 (BD Biosciences); F4/80-PE-Cy7 (eBiosience, San Diego, CA). Monocytes/macrophages were identified as CD11b^{hi} (CD90/B220/CD49b/NK1.1/Ly-6G)^{lo}. Neutrophils were identified as CD11b^{hi} (CD90/ B220/CD49b/NK1.1/Ly-6G)^{hi}. Data were acquired on an LSRII (BD Biosciences) with 670/LP and a 695/40 filter configuration to detect VT-680 on nanoparticles. The relative contribution of signal was calculated by multiplying the proportion of cells in the living cell gate by the mean fluorescent intensity. Data were analyzed using FlowJo v.8.5.2 (Tree Star, Inc.).

Statistics

Results are expressed as means ± SEM. Statistical comparisons between two groups were evaluated using the Mann Whitney test and ANOVA with Bonferroni post test was used for multiple comparisons. A value of $P < 0.05$ was considered to indicate statistical significance.

Results

Micro-CT imaging determines incidence, location and dimension of aortic aneurysms

The dimensions of aortic aneurysms were initially evaluated in wild type mice and in apoE$^{-/-}$ mice after AT-II administration, using contrast enhanced micro-CT. Supplementary Table 1 shows the intra- and interobserver variablity of the used CT angiography method. Aneurysm size was found to vary, ranging from 1.4 to 2.9 mm in diameter, with a mean of 1.8 mm (Table 1, Figure 1). Aneurysms were commonly observed in the ascending aorta,

and in the abdominal aorta. In two animals, more than one aortic aneurysm was found. Six mice died during the 28 day period of AT-II administration, and autopsy confirmed that aneurysm rupture was the cause of death. All but one mouse in this cohort developed aneurysms. The normal aortic diameter in the ascending aorta of wild type mice was 1.1 ± 0.1 mm, and was comparable to the diameter of non-dilated aortic sections in apoE$^{-/-}$ mice (Table 1). These sizes, location and incidence of rupture are consistent with prior work[15,16].

Dynamic PET-CT imaging to determine injection-imaging sequence

To determine the best imaging time point, a factor that is dependant on the *in vivo* biodistribution of the nanoparticle and on the decay of the PET reporter, we first performed dynamic PET imaging in 4 mice over several hours. Imaging was initially done between 2.5 to 6.5 hours following injection of the probe. During this time, the signal in blood was found to be consistantly higher than in the target region within the aortic wall. We therefore imaged from 9 to 13 hours after injection of the nanoparticle. Here, the blood pool signal dropped progessively. The 10–12 hour time point showed an optimal target-to-blood activity ratio, whilst activity of the PET isotope was still sufficient to provide a high number of counts. These in vivo findings were in line with the blood half life of ^{18}F-CLIO, which was determined by serial bleeds in a cohort of 4 wild type mice (Supplementary Figure 1). The mean blood half life estimated by monoexponential decay was 192 ± 14 min. Thus, all further imaging was done at 10–12 hours after injection of nanomaterials.

Macrophage-targeted PET imaging detects inflammation in AA

Nanoparticle uptake into the aortic wall was then quantified with PET, using CT images to guide placement of PET regions of interest. Significantly higher activities were found in the aneurysmal aortic sections (SUV are shown in Figure 2A, B). The target to blood backgound ratio in aneurysma was 2.4 ± 0.4, significantly higher than what was found in wild type aorta (0.7 ± 0.1, $p < 0.05$).

To compare the PET signal of aneurysm to atherosclerotic plaque, which also contains macrophages that may be targeted by ^{18}F-CLIO, we imaged a cohort of age-matched apoE$^{-/-}$ mice that were not implanted with AT-II delivering minipumps. Here, we found intermediate PET signal in aortic areas that are typically laden with atherosclerotic plaque. However, the uptake was significantly lower than in aneurysmal aorta (SUV aneurysma 2.5 ± 0.5 versus atherosclerotic plaque 1.2 ± 0.1, $p < 0.05$). Finally, these differences were also found when data were expressed as the target to blood ratio (1.3 ± 0.1, $p < 0.05$ versus aneurysm).

We also examined whether the aortic diameter measured by CT correlated with PET activity in the same vascular segment. Data pairs from aneurysms and non-aneurysmatic areas in apoE$^{-/-}$ mice were pooled and showed a weak correlation (Figure 2C, $R = 0.45$, $p < 0.05$).

Ex vivo scintillation counting and autoradiography confirm in vivo PET

To validate *in vivo* PET data, animals were sacrificed immediately after imaging and activity within excised aortas was assessed by scintillation counting and autoradiographic exposure. In comparison to wild type aortas, the percent injected radioactive dose per gram tissue increased in aortas with aneurysms (aneurysm 1.59 ± 0.18, non-aneurysmal aorta 0.87 ± 0.15, wild type aorta 0.52 ± 0.05, $p<0.05$ respectively, Figure 3A). Autoradiography showed that activity reached peak levels within the aneurysms, with some uptake also occurring in atherosclerotic plaques in the non-aneurysmatic vessel wall of apoE$^{-/-}$ mice (Figure 3B). By focusing on the fluorescent reporter on the nanoparticle, we also imaged aortas using a fluorescence reflectance microscope (Figure 3C) and found that fluorescence colocalized

with the ^{18}F signal. This demonstrated that the nuclear reporter and fluorochrome were still conjugated to the nanoparticle.

Microscopic nanoparticle signal colocalizes with macrophages in the aneurysm wall

Next, we studied the uptake of nanoparticles using microscopy (Figure 4). By comparing fluorescence microscopy images to immunohistochemistry staining for the macrophage antigen MAC-3 in adjacent sections, we found colocalisation of macrophages with nanoparticles in inflamed areas of the aneurysmatic wall. Macrophage presence as well as nanoparticle uptake was found in the intimal, medial, as well as in the adventitial layers of the aorta. Imaging of sections in the lower-wavelength fluoresceinthiocarbamyl (FTC) channel confirmed that the observed signal was specific to nanoparticles, and not caused by autofluorescence (Figure 4), and also demonstrated the disintegration of the tunica media, typically seen in aneurysms.

Cellular signal distribution by flow cytometry

We were also interested in quantitating uptake of nanoparticles by leukocyte populations (monocytes, macrophages, neutrophils and lymphocytes). To do this, we began by digesting aneurysmatic aortas following injection of the probe. We then studied the fluorescence signal derived from VT680 attached to the nanoparticles in cell suspensions that were stained for specific surface antigens of leukocytes. Using this method, we found that the majority of nanoparticles were taken up by monocytes/macrophages. Therefore, ~90% of the PET signal in aneurysms was caused by uptake of nanoparticles by these cells (Figure 5). Some, but much lower, uptake was also observed in neutrophils and lymphocytes (Figure 5). Administration of AT-II or mouse genotype did not change the uptake profile (Supplementary Figure 2).

Macrophage PET in nascent aneurysms

Our overall goal was to develop an imaging strategy that could detect inflammatory aneurysms before they rupture. If macrophage-targeted PET imaging is to be useful in the clinical setting, it would need to be able to detect inflammation in younger, evolving aneurysms. Therefore, we studied apoE$^{-/-}$ mice that had been exposed to AT-II administration for only 7 days. In these mice, we found that the PET signal was already significantly elevated (Figure 6A, B). The mean SUV of the aneurysms in these apoE$^{-/-}$ mice was 3.0 ± 0.4, compared to 0.82 ± 0.05 in wild type, and 2.46 ± 0.48 in the more mature aneurysms of apoE$^{-/-}$ mice that were imaged after 28 days of systemic AT-II exposure ($p<0.0001$ versus wild type). These imaging findings correlated well with the number of monocytes/macrophages in the vascular wall, as quantified by flow cytometry (Figure 6C). When compared to wild type, the monocyte/macrophage number in the aneurysmatic aortas of apoE$^{-/-}$ mice was increased 23-fold ($14.1 \times 10^4 \pm 5.5 \times 10^4$ versus $0.6 \times 10^4 \pm 0.4\ 10^4$). The profile of myeloid cells in the vessel also changed profoundly. In wild type mice, 80% of myeloid cells in the vessel wall were resident macrophages. However, in the wall of aortas with aneurysms, inflammatory Ly6C^{high} monocytes dominated this population (Figure 6C).

PET signal is decreased when inflammation is blunted

Next, the development of aneurysms and related PET signals were investigated in a group of mice that had undergone splenectomy at the time of AT-II minipump implantation. In a recent study, it was reported that the spleen contains a large reservoir of monocytes that significantly contribute to inflammation, and that release of this reservoir is triggered by AT-II signaling[17]. Since monocytes give rise to macrophages in tissue, we hypothesized that the splenic monocyte reservoir would contribute macrophages in our model of AA, and that

the removal of the splenic monocyte reservoir would decrease the number of macrophages in the aortic wall, reflected by a change of the PET signal. As expected, our results did indeed confirm this hypothesis and demonstrated that splenectomized mice had decreased PET signals in the aortic wall. The standard uptake value was reduced to 0.81 ± 0.11 ($p<0.05$ versus the signal from non-splenectomized apoE$^{-/-}$ mice). Importantly, these mice also displayed attenuated development of aneurysms under CT (only one aneurysm evolved, see also Table 1). Lastly, using flow cytometry, the number of monocytes/macrophages in the aorta of splenectomized mice was assessed and found to have a 3.8-fold reduction in number.

Predictive value of PET signal

Finally, we were interested in determining if macrophage targeted PET-CT had predictive potential. To this end, PET-CT imaging was performed on day 7 after implantation of AT-II minipumps, and mice were followed up by weekly serial CT angiography while the AT-II treatment was continued up to 4 weeks later. Of a total of 8 mice that underwent initial PET-CT, 3 mice died before completion of the study due to aneurysm rupture. In these mice and in mice with aneurysms that increased over time, the PET signal was increased when compared to aneurysms that did not increase in diameter on CT angiography follow-up (TBR 2.1 ± 0.3 versus 1.5 ± 0.1; $p < 0.05$, Figure 6D).

Discussion

The abundant presence and central role of macrophages in aneurysm formation[3,5,9,21] make them an interesting and clinically relevant imaging target. Experimental and clinical studies have shown that monocytes infiltrate the vessel wall, differentiate into macrophages and secrete inflammatory cytokines. In our study, using flow cytometry, we found an 18.6-fold increase in the population of macrophages present in aneurysms as compared to the aortic wall of control mice. Importantly, monocytes/macrophages are a major source for metalloproteinases and elastase, enzymes which degrade the media and thus reduce the tensile strength of the vascular wall[3,5,9]. These cells not only function as a major source of destabilizing enzymes but are also key instigators of further inflammation. Since aneurysm formation and progression is dependent on the strategic position of monocytes/macrophages, targeting these cells with imaging may offer early insight into the course of disease.

In this investigation, we used nanoparticles that are avidly internalized by phagocytic cells. The derivatization of these nanoparticles with ^{18}F allowed us to use PET imaging for *in vivo* macrophage detection. PET is a clinically attractive modality on account of its quantitative capabilities and its unsurpassed sensitivity. Indeed, this approach has enabled us to reduce the nanoparticle dose to clinically used levels (4.5 mg of iron oxide/kg body weight, which is lower than the recommended clinical dose for Feraheme©), encouraging translational pursuit since lower doses are associated with fewer side effects and less toxicity. We expect that the dose could be reduced further using next-generation macrophage PET agents, which would exploit variations in particle size so as to accelerate their redistribution from the blood pool to their target. These faster kinetics would also allow us to image at an earlier time point after injection, when less of the PET tracer has decayed. This advantage of more specific activity could then be used to decrease the agent dose. Alternatively, PET isotopes with longer half lives, such as copper-64 (^{64}Cu) or zirconium-89 (^{89}Zr) could be employed to image at later time points.

In the apoE$^{-/-}$ aneurysm model, we found a weak correlation between the aortic diameter measured by CT and the macrophage PET signal. Intriguingly, the PET signal was seen to be elevated relatively early in the course of the disease. This was demonstrated in animals that had only been exposed to AT-II for 7 days. In this cohort, the size of the aneurysms was

still increasing when compared to results from imaging sessions at later time points. These findings suggest that the use of macrophage-targeted imaging could be a valuable tool for assessing disease activity in nascent aortic aneurysms, supported by initial reports of ^{18}FDG-PET in patients with aortic disease[22–24].

Clinical management of aortic aneurysms is often faced with the important decision of whether to perform invasive repair, or whether a patient can be managed conservatively. The mortality rate associated with reparative surgery has been reported to be as high as 5.5%[25], but this is far exceeded by the mortality rate associated with aneurysm rupture[3]. Current guidelines[1,4] recommend endovascular repair or surgery if the aortic diameter exceeds 5.5 cm, and the performance of anatomic imaging every 3–6 months for aneurysms above 4 cm. If growth is observed to exceed 1 cm per year in smaller aneurysms, surgical repair is also recommended. However, individual risk is additionally influenced by gender, age, smoking and comorbidities, but its assessment is rarely easy since reliable data regarding how best to to evaluate these variables is not readily available[3]. This situation often leaves patients and doctors with a difficult decision, and many patients are unnecessarily exposed to the risks of reparative surgery when their aneurysm might never have ruptured if left untreated. An imaging approach that targets a key component of the biology underlying aneurysm rupture may help to more accurately determine individual risk as well as population-based risk factors. It is possible that a numerical cut-off SUV, determined by PET imaging, could be used as a decisive indicator for invasive repair, since underlying macrophage activity would be weakening the aneurysm wall. However, prospective outcome studies are needed, first in other preclinical models of aortic aneurysm, and eventually, after completion of toxicology studies, in patients. These trials will determine whether an increased macrophage PET signal, despite the limited spatial resolution of PET, can indeed predict aneurysm rupture.

Ultimately, we envision that imaging approaches, which target vascular biology[26–28] would be capable of identifying patients with rupture-prone aneurysms and who require surgical intervention. We also hope to accurately distinguish these patients early from patients with aneurysms that would be best served by watchful waiting strategies.

Supplementary Material

Refer to Web version on PubMed Central for supplementary material.

Acknowledgments

We gratefully acknowledge the help of Rostic Gorbatov, BS; Yoshiko Iwamoto, BS; Aleksey Chudnovskiy, MS; Brena Sena, BS; Won Woo Lee, MD PhD; Nikolay Sergeyev, PhD.

Funding Sources

This work was funded by grants from the NHI (Translational Program of Excellence in Nanotechnology UO1-HL080731/HHSN268201000044C, R24-CA92782 to RW, R01HL095629 and R01HL096576 to MN; R01HL095612 to FKS), AHA Established Investigator Award to REG and Deutsche Herzstiftung e. V. to FL.

References

1. Hirsch AT, Haskal ZJ, Hertzer NR, Bakal CW, Creager MA, Halperin JL, Hiratzka LF, Murphy WR, Olin JW, Puschett JB, Rosenfield KA, Sacks D, Stanley JC, Taylor LMJ, White CJ, White J, White RA, Antman EM, Smith SCJ, Adams CD, Anderson JL, Faxon DP, Fuster V, Gibbons RJ, Hunt SA, Jacobs AK, Nishimura R, Ornato JP, Page RL, Riegel B. ACC/AHA 2005 Practice Guidelines for the management of patients with peripheral arterial disease (lower extremity, renal, mesenteric, and abdominal aortic): a collaborative report from the American Association for Vascular Surgery/Society for Vascular Surgery, Society for Cardiovascular Angiography and

Interventions, Society for Vascular Medicine and Biology, Society of Interventional Radiology, and the ACC/AHA Task Force on Practice Guidelines (Writing Committee to Develop Guidelines for the Management of Patients With Peripheral Arterial Disease): endorsed by the American Association of Cardiovascular and Pulmonary Rehabilitation; National Heart, Lung, and Blood Institute; Society for Vascular Nursing; TransAtlantic Inter-Society Consensus; and Vascular Disease Foundation. Circulation. 2006; 113:e463–654. [PubMed: 16549646]

2. Dillavou ED, Muluk SC, Makaroun MS. A decade of change in abdominal aortic aneurysm repair in the United States: Have we improved outcomes equally between men and women? J Vasc Surg. 2006; 43:230–8. discussion 238. [PubMed: 16476592]
3. Brewster DC, Cronenwett JL, Hallett JWJ, Johnston KW, Krupski WC, Matsumura JS. Guidelines for the treatment of abdominal aortic aneurysms. Report of a subcommittee of the Joint Council of the American Association for Vascular Surgery and Society for Vascular Surgery. J Vasc Surg. 2003; 37:1106–1117. [PubMed: 12756363]
4. Chaikof EL, Brewster DC, Dalman RL, Makaroun MS, Illig KA, Sicard GA, Timaran CH, Upchurch GRJ, Veith FJ. The care of patients with an abdominal aortic aneurysm: the Society for Vascular Surgery practice guidelines. J Vasc Surg. 2009; 50:S2–49. [PubMed: 19786250]
5. Shimizu K, Mitchell RN, Libby P. Inflammation and cellular immune responses in abdominal aortic aneurysms. Arterioscler Thromb Vasc Biol. 2006; 26:987–994. [PubMed: 16497993]
6. Wang Y, Ait-Oufella H, Herbin O, Bonnin P, Ramkhelawon B, Taleb S, Huang J, Offenstadt G, Combadiere C, Renia L, Johnson JL, Tharaux PL, Tedgui A, Mallat Z. TGF-beta activity protects against inflammatory aortic aneurysm progression and complications in angiotensin II-infused mice. J Clin Invest. 2010; 120:422–432. [PubMed: 20101093]
7. Hellenthal FA, Buurman WA, Wodzig WK, Schurink GW. Biomarkers of abdominal aortic aneurysm progression. Part 2: inflammation. Nat Rev Cardiol. 2009; 6:543–552. [PubMed: 19546866]
8. Nahrendorf M, Pittet MJ, Swirski FK. Monocytes: protagonists of infarct inflammation and repair after myocardial infarction. Circulation. 2010; 121:2437–2445. [PubMed: 20530020]
9. Davies MJ. Aortic aneurysm formation: lessons from human studies and experimental models. Circulation. 1998; 98:193–195. [PubMed: 9697816]
10. Weissleder R, Kelly K, Sun EY, Shtatland T, Josephson L. Cell-specific targeting of nanoparticles by multivalent attachment of small molecules. Nat Biotechnol. 2005; 23:1418–1423. [PubMed: 16244656]
11. Nahrendorf M, Keliher E, Marinelli B, Waterman P, Feruglio PF, Fexon L, Pivovarov M, Swirski FK, Pittet MJ, Vinegoni C, Weissleder R. Hybrid PET-optical imaging using targeted probes. Proc Natl Acad Sci U S A. 2010; 107:7910–7915. [PubMed: 20385821]
12. Devaraj NK, Keliher EJ, Thurber GM, Nahrendorf M, Weissleder R. 18F labeled nanoparticles for in vivo PET-CT imaging. Bioconjug Chem. 2009; 20:397–401. [PubMed: 19138113]
13. Daugherty A, Manning MW, Cassis LA. Angiotensin II promotes atherosclerotic lesions and aneurysms in apolipoprotein E-deficient mice. J Clin Invest. 2000; 105:1605–1612. [PubMed: 10841519]
14. Daugherty A, Rateri DL, Cassis LA. Role of the renin-angiotensin system in the development of abdominal aortic aneurysms in animals and humans. Ann N Y Acad Sci. 2006; 1085:82–91. [PubMed: 17182925]
15. King VL, Lin AY, Kristo F, Anderson TJ, Ahluwalia N, Hardy GJ, Owens APr, Howatt DA, Shen D, Tager AM, Luster AD, Daugherty A, Gerszten RE. Interferon-gamma and the interferon-inducible chemokine CXCL10 protect against aneurysm formation and rupture. Circulation. 2009; 119:426–435. [PubMed: 19139386]
16. Barisione C, Charnigo R, Howatt DA, Moorleghen JJ, Rateri DL, Daugherty A. Rapid dilation of the abdominal aorta during infusion of angiotensin II detected by noninvasive high-frequency ultrasonography. J Vasc Surg. 2006; 44:372–376. [PubMed: 16890871]
17. Swirski F, Nahrendorf M, Etzrodt M, Wildgruber M, Cortez-Retamozo V, Panizzi P, Figueiredo J, Kohler R, Chudnovskiy A, Waterman P, Aikawa E, Mempel T, Libby P, Weissleder R, Pittet M. Identification of Splenic Reservoir Monocytes and Their Deployment to Inflammatory Sites. Science. 2009; 325:612–616. [PubMed: 19644120]

18. Leuschner F, Panizzi P, Chico-Calero I, Lee WW, Ueno T, Cortez-Retamozo V, Waterman P, Gorbatov R, Marinelli B, Iwamoto Y, Chudnovskiy A, Figueiredo JL, Sosnovik DE, Pittet MJ, Swirski FK, Weissleder R, Nahrendorf M. Angiotensin-converting enzyme inhibition prevents the release of monocytes from their splenic reservoir in mice with myocardial infarction. Circ Res. 2010; 107:1364–1373. [PubMed: 20930148]
19. Visser EP, Disselhorst JA, Brom M, Laverman P, Gotthardt M, Oyen WJ, Boerman OC. Spatial resolution and sensitivity of the Inveon small-animal PET scanner. J Nucl Med. 2009; 50:139–147. [PubMed: 19139188]
20. Nahrendorf M, Swirski FK, Aikawa E, Stangenberg L, Wurdinger T, Figueiredo JL, Libby P, Weissleder R, Pittet MJ. The healing myocardium sequentially mobilizes two monocyte subsets with divergent and complementary functions. J Exp Med. 2007; 204:3037–3047. [PubMed: 18025128]
21. Tieu BC, Lee C, Sun H, Lejeune W, Recinos Ar, Ju X, Spratt H, Guo DC, Milewicz D, Tilton RG, Brasier AR. An adventitial IL-6/MCP1 amplification loop accelerates macrophage-mediated vascular inflammation leading to aortic dissection in mice. J Clin Invest. 2009; 119:3637–3651. [PubMed: 19920349]
22. Truijers M, Kurvers HA, Bredie SJ, Oyen WJ, Blankensteijn JD. In vivo imaging of abdominal aortic aneurysms: increased FDG uptake suggests inflammation in the aneurysm wall. J Endovasc Ther. 2008; 15:462–467. [PubMed: 18729562]
23. Reeps C, Essler M, Pelisek J, Seidl S, Eckstein HH, Krause BJ. Increased 18F-fluorodeoxyglucose uptake in abdominal aortic aneurysms in positron emission/computed tomography is associated with inflammation, aortic wall instability, and acute symptoms. J Vasc Surg. 2008; 48:417–23. discussion 424. [PubMed: 18572354]
24. Xu XY, Borghi A, Nchimi A, Leung J, Gomez P, Cheng Z, Defraigne JO, Sakalihasan N. High levels of 18F-FDG uptake in aortic aneurysm wall are associated with high wall stress. Eur J Vasc Endovasc Surg. 2010; 39:295–301. [PubMed: 19926315]
25. Hallin A, Bergqvist D, Holmberg L. Literature review of surgical management of abdominal aortic aneurysm. Eur J Vasc Endovasc Surg. 2001; 22:197–204. [PubMed: 11506510]
26. Nahrendorf M, Sosnovik DE, French BA, Swirski FK, Bengel F, Sadeghi MM, Lindner JR, Wu JC, Kraitchman DL, Fayad ZA, Sinusas AJ. Multimodality cardiovascular molecular imaging, Part II. Circ Cardiovasc Imaging. 2009; 2:56–70. [PubMed: 19808565]
27. Sanz J, Fayad ZA. Imaging of atherosclerotic cardiovascular disease. Nature. 2008; 451:953–957. [PubMed: 18288186]
28. Tedesco MM, Terashima M, Blankenberg FG, Levashova Z, Spin JM, Backer MV, Backer JM, Sho M, Sho E, McConnell MV, Dalman RL. Analysis of in situ and ex vivo vascular endothelial growth factor receptor expression during experimental aortic aneurysm progression. Arterioscler Thromb Vasc Biol. 2009; 29:1452–1457. [PubMed: 19574559]

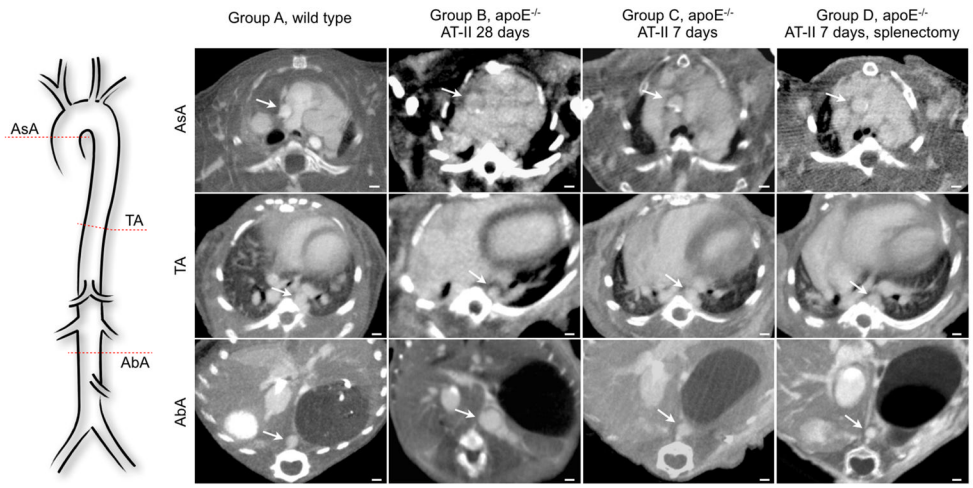

Figure 1. CT angiography

CT angiography in experimental groups. The dotted circles outline the short axis view of the aorta. The circles are of equal size, and the distance bar denotes 1 mm. Diameter data are listed in Table 1. AsA: Ascending aorta, TA: thoracic aorta, AbA: abdominal aorta.

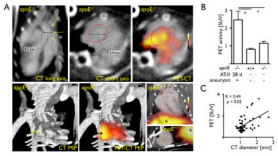

Figure 2. Macrophage-PET in mice with aortic aneurysm

PET-CT imaging in mice with aortic aneurysms. **(A)** Representative PET-CT images. Yellow arrows and dotted lines outline the aneurysmatic aorta. MIP: Maximum intensity projection. * denotes liver signal. **(B)** *In vivo* PET signal derived from the aneurysmatic vessel wall at the site of the aneurysm (left) wild type controls (middle), and apoE$^{-/-}$ mice that did not receive AT-II (right bar). SUV: standard uptake value. Data are presented as mean ± SEM, * $p < 0.01$. **(C)** A correlation of the PET signal with aortic diameter (measured by CT), after AT-II delivery in apoE$^{-/-}$ mice. PET signal and diameter were measured in aneurysmatic and normal section of the aorta in apoE$^{-/-}$ mice exposed to AT-II. It is possible that in some cases, these sections may have contained atherosclerotic plaques that had not been detected by CT.

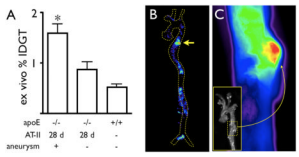

Figure 3. *Ex vivo* validation of PET signal

Ex vivo imaging, 28 days after AT-II administration. **(A)** Scintillation counting of excised aortic sections served to corroborate results from *in vivo* PET-CT imaging. Data are normalized for weight, decay and injected activity, and presented as mean ± standard error, * $p < 0.01$. **(B)** Autoradiography of an aneurysm in the descending thoracic aorta (arrow). Some activity, albeit at a lower level, was also observed in distal aortic segments. Whilst these segments contained small atherosclerotic plaques, they were not dilated. **(C)** A fluorescence reflectance image of the same aorta. The inset depicts a white light image. Nuclear and optical imaging concordantly showed nanoparticle accumulation in the aneurysmatic vessel wall.

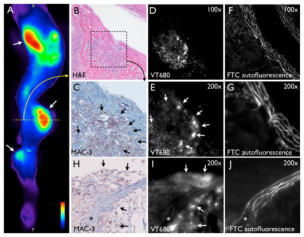

Figure 4. Microscopic agent distribution

Histology from an aneurysmatic aorta after 28 days of AT-II administration. **(A)** A fluorescence image showing nanoparticle accumulation in the aneurysm wall (arrows). The dotted line indicates the approximate location of the histological sections. **(B)** H&E histology, magnification 100×. **(C, H)** Immunohistochemistry indicating the presence of macrophages (arrows), magnification 200×. The vessel lumen is located in the upper part of the image. **(D, E, I)** Fluorescence images depicting nanoparticle distribution (arrows) in an adjacent section, magnification 100 (D) and 200× (E, I). While there is some accumulation in macrophages in luminal atherosclerotic plaque, robust signal is located in adventitial macrophages next to degraded media (asterisk in H-J). **(F, G, J)** Autofluorescence images of the aorta, magnification 100 and 200×, respectively.

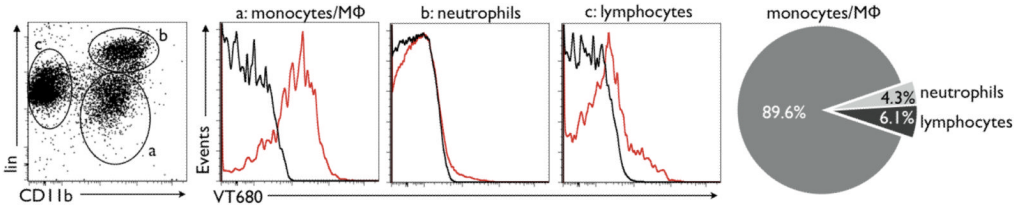

Figure 5. Quantitation of cellular signal contribution

Flow cytometric analysis of digested aortas. Mice with aneurysms were injected with nanoparticles 12 hours prior to analysis. The plot on the far left shows the leukocyte populations present: monocytes/macrophages in gate (a), neutrophils in gate (b), and lymphocytes in gate (c). The three successive histograms depict their respective intracellular signals in the VT680 channel, which reports on nanoparticle uptake by the cells. The black line indicates the signal in cells of a non-injected mouse (controlling for background autofluorescence), while the red line represents the signal from cells retrieved from an aneurysmatic aorta of an apoE$^{-/-}$ mouse after injection of the probe. The pie chart on the far right depicts the relative signal contribution per cell type, relative to the overall signal in apoE$^{-/-}$ mice. Of note, this analysis only accounts for intracellular nanoparticles.

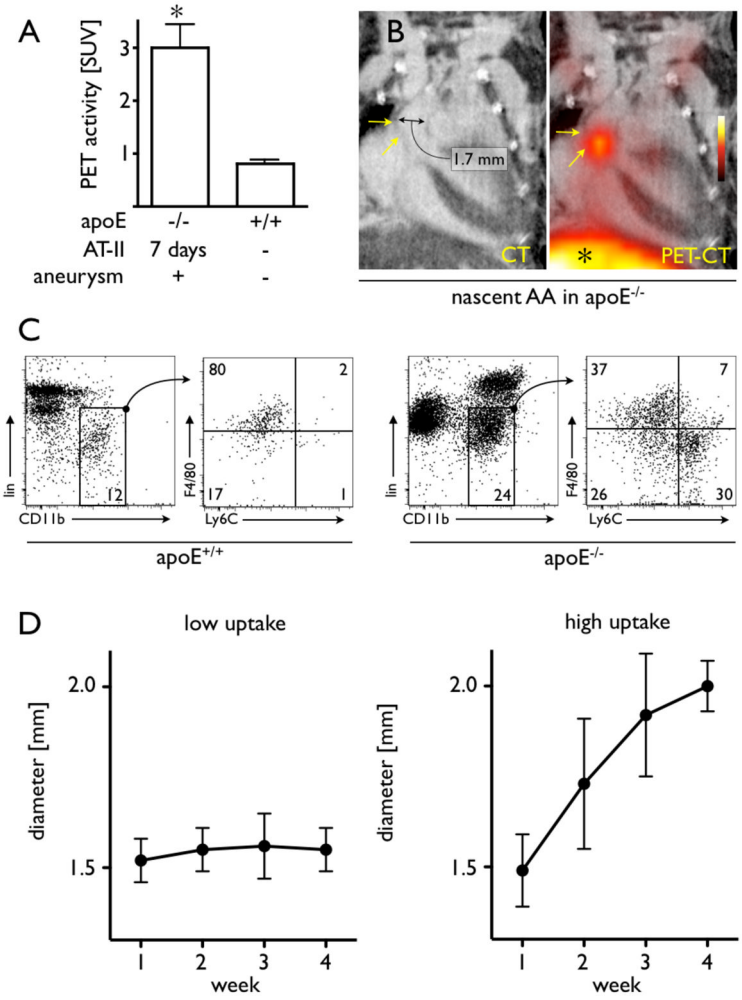

Figure 6. Macrophage-PET in nascent aneurysms

Imaging in mice with early-stage aneurysms (undergoing 7 days of AT-II administration). **(A)** PET signals from aneurysms and from wild type mice. Data are presented as mean ± standard error. * indicates $p<0.05$. SUV: standard uptake value. **(B)** Representative PET-CT images of a nascent aortic aneurysm (AA), * indicates liver signal. **(C)** Flow cytometric analysis of leukocytes in the aorta of wild type mice (left two plots) and apoE$^{-/-}$ mice (right two plots) after 7 days of AT-II administration. The gated regions in the left plots for each mouse type depict the monocyte/ macrophage population, which were further analyzed for expression of the monocyte surface marker Ly6-C and the macrophage marker F4/80 (plots on the right). Lin: lineage antigens (CD90/B220/CD49b/NK1.1/Ly-6G). Numbers contained within the gated regions of the plots (left plots) indicate percentage of living cells (macrophages/monocytes). Numbers in the quadrants (right plots) indicate the percentage of monocytes/macrophages in each gate. **(D)** Serial CT angiography after PET-CT on day 7 in AT-II treated apoE$^{-/-}$ mice. Left panel shows the diameter of aneurysms with low PET signal (PET TBR 1.5 ± 0.1), right panel shows diameter of aneurysms with high signal (2.1 ± 0.3; $p < 0.05$ versus low uptake). Diameter is displayed as mean ± SEM.

Table 1

Model characteristics

The number of animals used, mortality and aortic diameter (assessed by micro-CT imaging). The spatial resolution of CT was 60μm isotropically

	group	n	AA - related deaths	deaths [%]	diameter [mm]			
					aneurysm	ascending aorta	descending thoracic aorta	abdominal aorta
A	wild type	10	0	0	n. a.	1.07 ± 0.03	1.07 ± 0.03	1.07 ± 0.07
B	apoE$^{-/-}$ AT-II 28 days	16	6	37.5	1.85 ± 0.08*	1.25 ± 0.03	1.14 ± 0.04	1.16 ± 0.06
C	apoE$^{-/-}$ AT-II 7 days	6	1	17	1.64 ± 0.08*	1.15 ± 0.08	1.11 ± 0.09	0.96 ± 0.11
D	apoE$^{-/-}$ AT-II 7 days splenectomy	5	0	0	1.50	1.12 ± 0.06	1.00 ± 0.02	1.00 ± 0.07

Data are presented as mean ± standard error,

* $p < 0.01$ versus wild type and non-aneurysmatic sections.